Spring 5-1-2022

Triggering Thermal Runaway in Lithium-ion Batteries

Chris John
cjohn64@outlook.com

Honors Thesis

May 2022

TRIGGERING THERMAL RUNAWAY IN LITHIUM-ION BATTERIES

Chris John

Honors Advisor: Dr. Jason Lee

Thesis Supervisor: Dr. Wilson K. S. Chiu

School of Engineering, Department of Mechanical Engineering

i Abstract

The proliferation of lithium-ion batteries (LIBs) has become significant. LIBs allow innumerable technological advances such as smartphones, laptops, and many other electronic devices to see widespread use. The same advances in LIB technology have allowed electric vehicles to become a reality into the 21st century. Their use is not without fault, however, as a latent and extreme danger exists in all LIBs. An external stimulus such as physical damage, overcharging, or elevated temperature can cause LIBs to undergo a phenomenon known as thermal runaway (TR). TR is characterized by a rapid increase in battery temperature due to a cascade of decomposition reactions, potentially leading to complete combustion of the battery. A battery reaching this point can prove catastrophic to personal safety and property. There is therefore a need to improve battery safety in this field.

The damage mechanisms mentioned – physical damage, overcharging, and elevated temperature – trigger TR by forcing an internal short circuit (ISC) between the internal layers of a battery. This initiates a series of decomposition reactions within the battery layers, leading to immense heat release and a potential fire. If one cell undergoes TR in a multicell array, it is possible for other nearby cells to undergo TR as well, presenting a significant safety flaw. While newer batteries are being designed with improved safety methods for specific use cases, there is not a generalized model allowing for quick and accurate modeling of a battery holder which can prevent propagation of TR to other cells. This research project saw the development of a computational model simulating TR in a single cell as well as the development of a generalized, scalable battery holder which can prevent TR from spreading to other cells. This model allows for material properties, dimensions, and other parameters to be varied and evaluated depending on the use case. The application in which the batteries are to be used will influence the battery holder parameters.

COMSOL Multiphysics is a Finite Element Analysis (FEA) program used for developing these models. An average-property model (APM) of an 18650 cell was created based on literature to establish a basis model to obtain temperature and heat release data. TR was successfully triggered in this single cell using a heater with a specified heat input to simulate the breakdown of internal battery layers. The 18650 model laid the groundwork upon which mitigation techniques can be evaluated. A generalized battery case called

the honeycomb was modeled and allows for seven 18650 cells to be inserted. The scalable geometry of this battery holder allows it to hold as many cells as needed. The parameters of this case such as materials and dimensions were varied to determine the best ways to passively prevent TR propagation in multicell arrangements.

Table of Contents

Table of Figures

Table of Tables

ii Glossary

Acronym	Term
APM	Average-property model
DAE	Differential-algebraic system of equations
EV	Electric vehicle
HPC	High performance computing
ISC	Internal short circuit
LCO	Lithium cobalt oxide
LIB	Lithium-ion battery
ne/NE	Negative electrode
ODE	Ordinary differential equation
pe/PE	Positive electrode
SEI	Solid electrolyte interface
TR	Thermal runaway

iii Nomenclature

Variable	Unit	Meaning
A	[1/s]	Frequency factor (pre-exponential term in Arrhenius equation)
c		Concentration
E_a	[J/mol]	Activation energy
H	[J/kg]	Specific enthalpy
h	$\mathrm{W/(m^2K)}$	Convection coefficient
k	[W/(mK)]	Thermal conductivity
k	[1/s]	Reaction rate)
m		Reaction order
q	[W]	Rate of heat transfer
q''	$[\mathrm{W/m^2}]$	Heat flux
Q	$[\mathrm{W/m^3}]$	Volumetric heat generation
R	$[\mathrm{J/(mol \cdot K)}]$	Universal gas constant
t	[mm]	Thickness
T	[°C]	Temperature
W	$[\mathrm{kg/m^3}]$	Specific reactive content
α		Concentration
α	$[\mathrm{m^2/s}]$	Thermal diffusivity
κ	$[\mathrm{W/(m \cdot K)}]$	Thermal conductivity tensor
σ	5.67×10^{-8} $[\mathrm{W/(m^2 \cdot K^4)}]$	Stefan–Boltzmann constant

1 Research Overview

1.1 The Thermal Runaway Process

TR is a positive-feedback loop initiated due to damage to a battery. Physical damage, overheating, or overcharging a battery can cause an internal short circuit (ISC) between the inner battery layers shown in figure 1. These layers are briefly summarized in table 1. Short circuits are characterized by high currents with minimal resistance, and this causes some heat generation due to Joule heating. The amount of heat released depends on the type of short circuit, with type c being the most severe. The high electrical conductivities of the aluminium current collector and graphite anode decreases electrical resistance, leading to increased current in an already high short circuit situation such as that in a type c ISC. Normally this heat dissipates to the environment, but since the heat is trapped within the enclosed volume of the battery, it triggers temperature-dependent decomposition reactions should the ISC generate enough heat. Highly reactive material resides within these battery layers and especially within the electrodes and electrolyte materials. These decomposition reactions release even more heat, increasing the temperature and increasing the rate of the decomposition reactions further. A point is reached where the temperature and heat generation spike greatly. This is typically the point where the battery catches fire, after which the reactant material is largely burned off.

TR is typically spontaneous with multiple outcomes possible. The decomposition reactions can remain slow enough such that the heat release is spread over a long duration. This would prevent further decomposition reactions from initiating. The battery would cease to function but would not catch fire, limiting potential damage. However, it is also possible these reactions onset quickly and the entire battery combusts in seconds. This is depicted in a nail penetration test with the resulting fire shown in figure 2. This test simply drives a nail through the battery, causing an ISC within the battery. While the decomposition reactions increase the battery temperature, the resulting fire emerges within just milliseconds in this test. These situations can trigger nearby batteries to under TR as well.

1.2 Research Objectives and Deliverables

LIB applications are limitless, and each application demands a specific method by which to contain batteries. However, there is currently no standardized or generalized model for containing batteries – it is application-dependent. Many computational models are specific to already-developed experimental procedures or production models of battery holders. These models cannot be readily adapted for different applications outside of the specific application on which it is based. There is a need to generalize this pro-

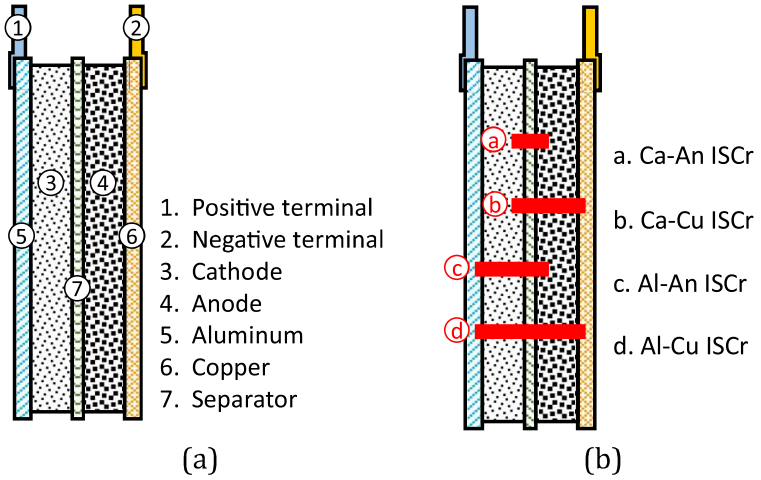

Figure 1: Major components of an LIB and the possible types of short circuits [7]

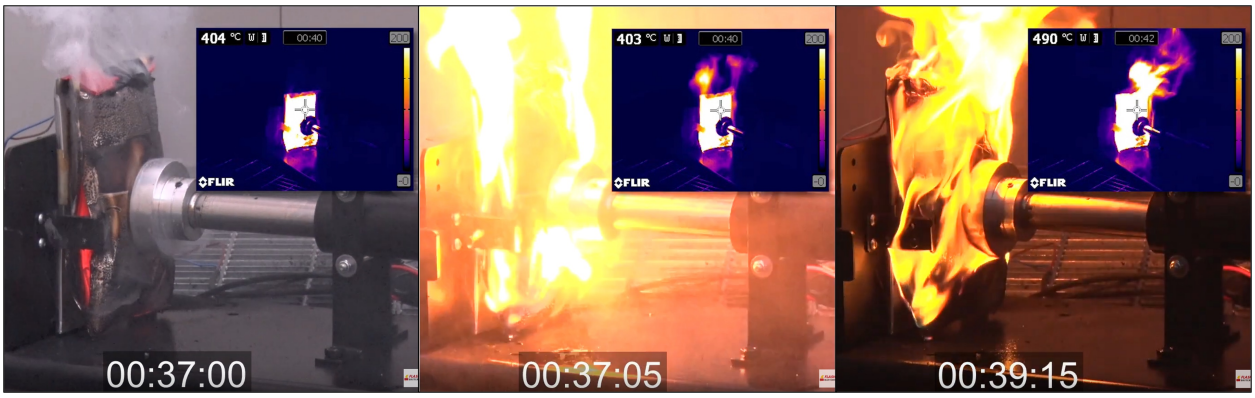

Figure 2: Depiction of TR in a nail penetration test [1] – the battery is engulfed in flames in seconds

Layer	Function	Material
Positive current collector	Receives electrons during discharge from the negative current collector	Aluminum
Cathode	Stores Li-ions and releases them when the battery is charging	Intercalated Li compound
Electrolyte	Medium through which Li-ions travel	Ether (varies)
Separator	Blocks electrons but allow ions to pass through	Varies, typically a polyolefin (polyethylene or polypropylene)
Anode	Stores Li-ions and releases them when discharging	Graphite
Negative current collector	Receives electrons during charging from positive current collector	Copper

Table 1: Layers, general functions, and typical materials within LIBs

cess and understand not only the thermal characteristics of TR, but also how to prevent TR propagation to other cells in multicell arrangements. While experimental procedures exist for evaluating TR, capturing data can be challenging and costly. There also exists a great environmental, health, and safety hazard with the intentional destruction of LIBs. This research focused on producing computational models of TR which can be applied to generalized applications. These computational models rely on established decomposition reactions combined with parameters for typical LIBs. This allows confidence in the models without the need for hazardous or costly experimental setups. Applying these to a single cell battery will allow collection of battery temperature and heat generation data for common battery form factors. This single cell model can then be used in the development of a battery holder to assess if the battery holder can prevent TR from propagating to other cells.

The overarching scope of this project is improving battery safety by developing computational models to better understand TR in single cell and multicell arrangements. Two primary objective are outlined to reinforce this understanding. The first objective was triggering TR in a single 18650 cell. These are cylindrical batteries measuring 18 mm in diameter and 65.0 mm in height. A simplified diagram is shown in 4 and is explained further in later sections. These batteries are used in applications ranging from flashlights, small battery banks for mobile devices, and more recently, electric vehicles (EVs). A FEA program can then be used to obtain temperature and heat generation/release data.

The second objective is developing a generalized battery holder. This battery holder must be scalable to fit different applications. An EV, for instance, demands thousands of cells subject to the forces of driving, while a backup battery for a computer may demand tens or hundreds of cells and may only deal with the occasional bump or minor drop. The holder model should be readily adaptable to this wide range of applications. This means the battery holder must be parameterized so dimensions, materials, and cell arrangements can be changed quickly. Dimensions and other properties should not be constants, but rather be allowed to vary to assess how changing properties affect the cells inside. The battery separation distances, height of the case, length of side walls, and other variables should be defined by functions which can be readily inputted into COMSOL.

While not necessary to recreate a time-dependent accurate simulation, it is important for temperature and heat generation data to be accurate. These two data points are the most crucial for preventing TR propagation. Validation with literature and video content proves necessary to ensure an accurate model is developed. Video content involves experiments which trigger TR and measure battery temperature through infrared cameras or by other means. While not an accurate method to assess accuracy, it provides a rough range of acceptable temperatures to determine if the basis 18650 model is sufficient for future work.

The ubiquitous nature of LIBs means the general public becomes a significant benefactor in this research.

Successful results are crucial for the improvement of battery safety in a wide range of applications. TR occurring in EVs, which contain thousands of battery cells, can prove catastrophic to drivers, passengers, property, and the environment. The completion of these two objectives provide an essential component for ongoing advances in battery safety.

1.3 Need for Battery Safety

LIB are used in limitless applications. They see use in everything from headsets to EVs and even whole-house backup batteries. These applications require an immense number of battery cells and contribute to the exponential increase in demand as seen in figure 3. Bloomberg New Energy Finance (NEF) published this figure to highlight not only battery demand increases but where demand will increase the most [3]. A significant rise in demand is expected in the transportation sector, which presents a serious need to guarantee battery safety. These are applications which present the greatest risk to environmental, health, and safety factors.

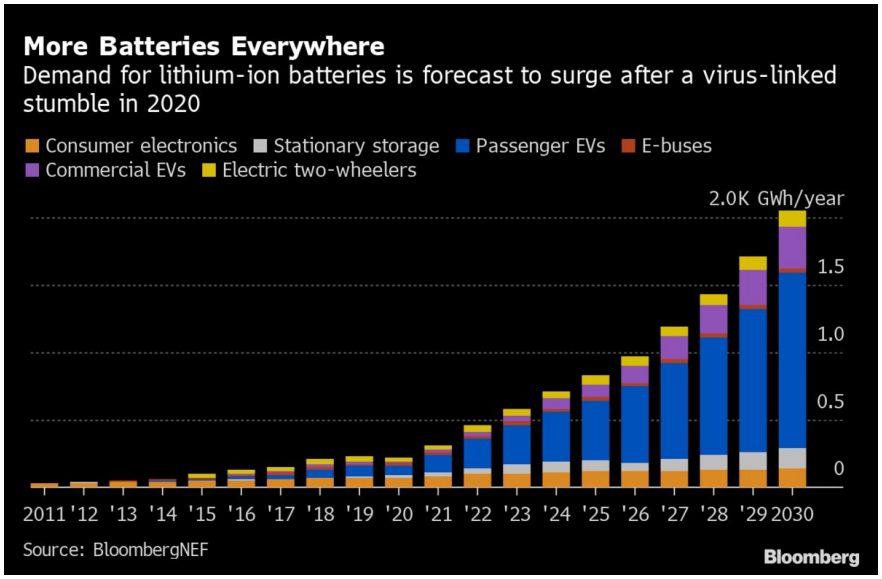

Figure 3: Projected battery demand over the next decade

Improving battery safety will ensure consumers and the broader market will be prepared to deal with an immense increase in LIB demand and proliferation. It is imperative generalized safety methods of containing battery cells are developed as demand will only increase.

2 Modeling TR in a Single 18650 Cell

2.1 Physical Model Parameters

Modeling TR relies on first choosing a common battery form factor and chemistry. 18650 cells, as described before, are used in many applications from flashlights to EVs. Multiple battery cathode materials exist, so it is also necessary to first select a cathode material as this will influence input parameters used in COMSOL. Lithium-cobalt-oxide ($LiCoO_2$) is a common cathode material in LIBs and is the cathode material of choice used for this research. The model is a simple cylindrical, average-property model (APM) depicted in figure 4 and shown in detail in figure 6. An APM is necessary to avoid modeling issues arising from modeling the thin, internal layers of a cylindrical battery as shown in figure 5. This would introduce unnecessary complexity and severely impact computation times.

Only relevant thermal properties are needed for the APM. This includes the density, thermal conductivity, and specific heat (ρ, k, c_p, respectively). The properties of each of the materials within the battery are averaged together, and the volume those components occupy acts as a weight for calculating the average. Since the length and width of the layers are the same when they are rolled up in the battery, only the thickness is needed as a weight. Density and specific heat are isotropic, and thermal conductivity is calculated in an orthotropic manner using equation 1 to obtain the through-plane and in-plane values. The properties of the heater and battery are shown in table 2.

$$k_{\parallel} = \frac{\sum_i k_i d_i}{\sum_i d_i} \qquad\qquad k_{\perp} = \frac{\sum_i d_i}{\sum_i d_i / k_i} \tag{1}$$

Table 2: Table of properties in common between all current models

	k [W/mK]	c_p [J/kgK]	ρ [kg/m^3]
Battery	34 in-plane ($k_{\parallel}$) 3.4 thru-plane ($k_{\perp}$)	830	1700
Heater	44.5	475	7850

The simplest method by which to trigger TR in a computational setting is a thermal input. This simulates a TR event caused by an external heat source increasing the temperature enough to trigger the decomposition reactions in the battery. The heater shown in orange is modeled as a constant heat source outputting 40 W of heat into the battery – this is in direct contact with the battery. All battery and heater surfaces are adiabatic so no heat is lost to the environment. This depicts a scenario in which the battery cannot remove

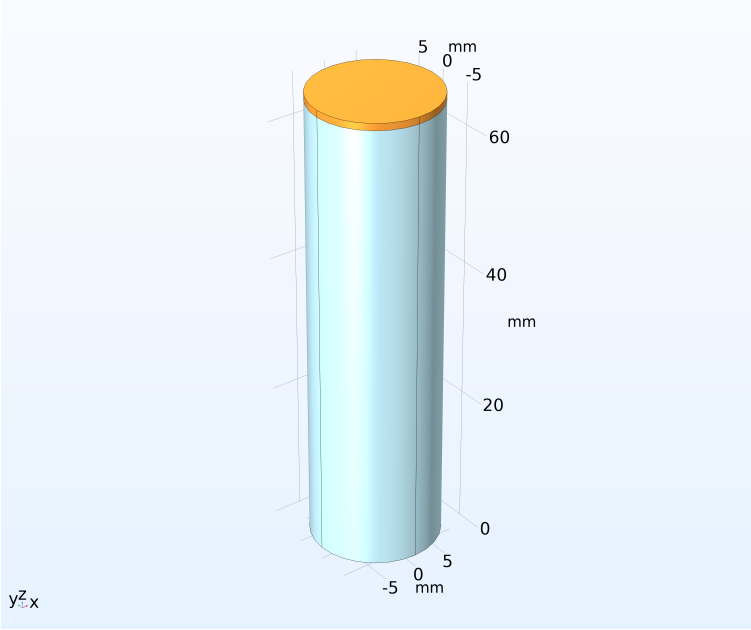

Figure 4: Model of a single 18650 cell as it appears in COMSOL. A heater (orange) is placed on top.

heat to prevent TR – a worst-case scenario in LIB safety. This simulation is run for 60 s and data is saved at a rate of 100 Hz. This data rate is sufficient for capturing the characteristic temperature spike seen in TR events. The relative and absolute solver tolerances were set to 10^{-6} and 10^{-8}, respectively. Such a low solver tolerance is necessary to ensure high solving accuracy especially when the temperature spike occurs. COMSOL automatically determines the proper time steps according to these tolerances. A low tolerance is necessary to ensure the TR temperature spike is properly captured as it occurs over the space of a few milliseconds. Modeling TR can now proceed with the selected from factor and chemistry.

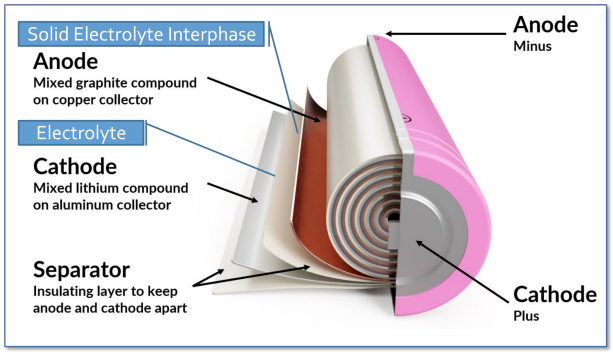

Figure 5: Simplified model of a typical cylindrical battery with relevant components labeled

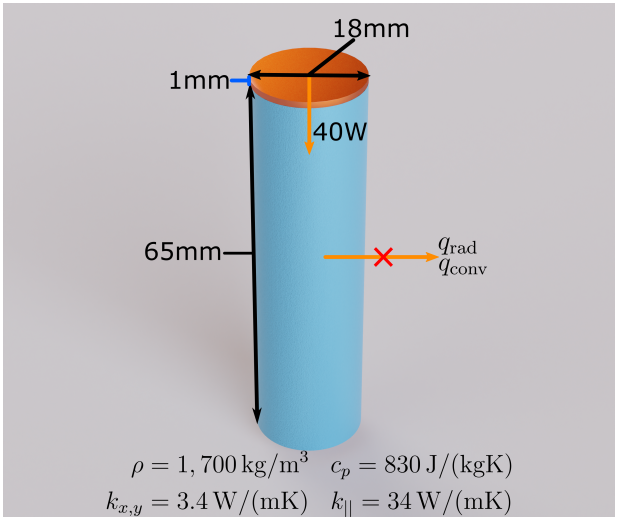

Figure 6: Diagram of the 18650 cell summarizing dimensions, properties, and boundary conditions

2.2 Analytical Functions

Modeling TR relies on solving a set of equations not available in FEA packages. These equations must be manually input to calculate the total heat inputted and generated within the model. The FEA program (COMSOL Multiphysics in this case) then obtains temperature data from the heat generated. The first equation input is the total heat generated in a TR event depicted by equation 2:

$$Q_{\text{tot}} = \sum Q_i = Q_{\text{sei}} + Q_{\text{ne}} + Q_{\text{pe}} + Q_{\text{e}} + Q_{\text{in}} \tag{2}$$

where Q_{sei}, Q_{ne}, Q_{pe}, and Q_{e} describe the heat generated from the decomposition of the solid electrolyte interface (SEI), the negative electrode (NE), the positive electrode (PE) and the electrolyte (E), respectively. Q_{in} describes the heat input from the heater placed on top of the battery. The four heat generation terms are Arrhenius-based, time and temperature-dependent equations described by equations 3–6:

$$Q_{\text{sei}} = H_{\text{sei}} W_c c_{\text{sei}}^{m_{\text{sei}}} A_{\text{sei}} \exp\left(\frac{-E_{a,sei}}{RT}\right) \tag{3}$$

$$Q_{\text{ne}} = H_{\text{ne}} W_c c_{\text{ne}}^{m_{\text{ne}}} \exp\left(\frac{-t_{\text{sei}}}{t_{\text{sei},0}}\right) A_{\text{ne}} \exp\left(\frac{-E_{a,ne}}{RT}\right) \tag{4}$$

$$Q_{\text{pe}} = H_{\text{pe}} W_p \alpha^{m_{\text{pe,p1}}} (1-\alpha)^{m_{\text{pe,p2}}} A_{\text{pe}} \exp\left(\frac{-E_{a,pe}}{RT}\right) \tag{5}$$

$$Q_{\text{e}} = H_e W_e c_e^{m_e} A_e \exp\left(\frac{-E_{a,e}}{RT}\right) \tag{6}$$

where H is specific enthalpy, W is specific content of a substance (subscript c is for carbon, p is for positive active content, e is for electrolyte content), c and α denote concentrations of substances, A is the Arrhenius equation pre-exponential term, E is activation energy, and t denotes the SEI thickness. There are five unknowns within these four equations (four concentrations and SEI thickness), which must be obtained by numerically solving five differential equations. Equations 7–11 describe the rates at which these variables change. These differential equations appear in the heat generation equations outlined before. Finally, figure 7 shows a flowchart of how the total heat generation is computed. This process must be set up using the

ODE and DAE interface in COMSOL.

$$\frac{dc_{\text{sei}}}{dt} = -A_{\text{sei}} \exp\left(-\frac{E_{\text{a,sei}}}{RT}\right) c_{\text{sei}}^{m_{\text{sei}}} \tag{7}$$

$$\frac{dc_{\text{ne}}}{dt} = -A_{\text{ne}} \exp\left(-\frac{E_{\text{a,ne}}}{RT}\right) \exp\left(-\frac{t_{\text{sei}}}{t_{\text{sei0}}}\right) c_{\text{ne}}^{m_{\text{ne}}} \tag{8}$$

$$\frac{dt_{\text{sei}}}{dt} = A_{\text{ne}} \exp\left(-\frac{E_{\text{a,ne}}}{RT}\right) \exp\left(-\frac{t_{\text{sei}}}{t_{\text{sei0}}}\right) c_{\text{ne}}^{m_{\text{ne}}} \tag{9}$$

$$\frac{d\alpha}{dt} = A_{\text{pe}} \exp\left(-\frac{E_{\text{a,pe}}}{RT}\right) \alpha^{m_{\text{pe,p1}}} (1-\alpha)^{m_{\text{pe,p2}}} \tag{10}$$

$$\frac{dc_e}{dt} = -A_e \exp\left(-\frac{E_{\text{a,e}}}{RT}\right) c_e^{m_e} \tag{11}$$

The initial rates of change are all set to 0 and the parameters outlined in table 5 are input to the equations. Another needed input is the temperatures at which the decomposition reactions start – these are shown in table 3. When the maximum temperature seen in the model reaches these temperatures, the decomposition respective reaction "switches on" and starts contributing to the total heat term seen in equation 2. Each reaction releases an amount of energy proportional to the specific enthalpy, so this must be input as well. The simulation is now ready to run as the geometry, inputs, and equations are all defined.

Reactions	Onset T [°C]	ΔH [J/g]
SEI Decomposition	60	273
Anode Decomposition	120	1714
Separator Melting	120	23
Cathode Decomposition	240	314
Electrolyte Decomposition	250	155

Table 3: Initiation temperatures and specific enthalpies for Li-ion battery TR events

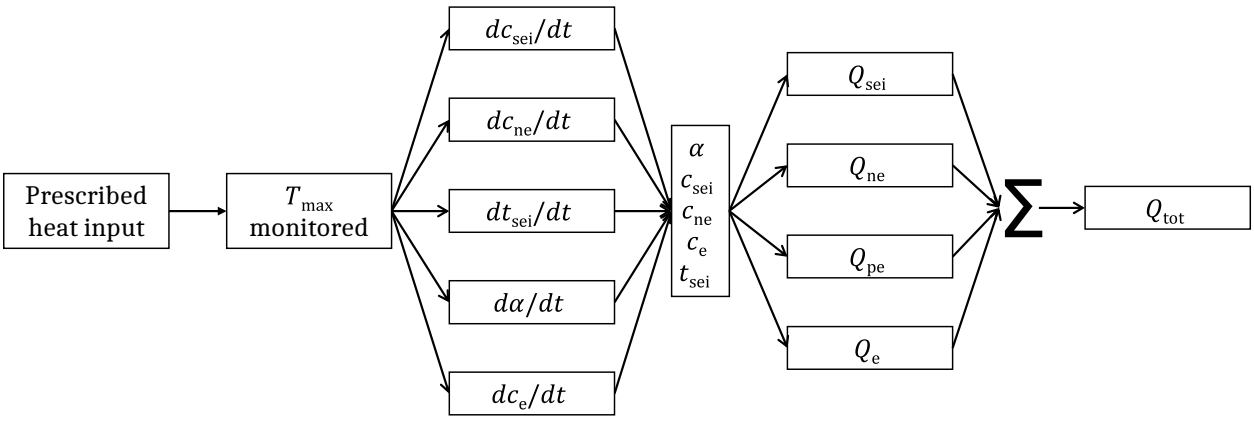

Figure 7: Flowchart showing how decomposition heat generation is calculated

2.3 Results: Single Cell TR Model

Data collected from the single 18650 model includes the maximum temperature, average temperature over the entire battery volume, and the volumetric heat generated from the decomposition reactions. This data is plotted in figures 8–12. Temperature data is calculated in COMSOL directly, while the volumetric heat generation is calculated using equation 2. Q_{tot} can be found at any time since COMSOL solves for these equations, so this data can be plotted as shown in figure 9. The heater is not considered in the maximum temperature, average temperature, or heat generation calculations, however. This ensures the battery is the only object being analyzed – including the heater would lead to inaccurate heat generation data.

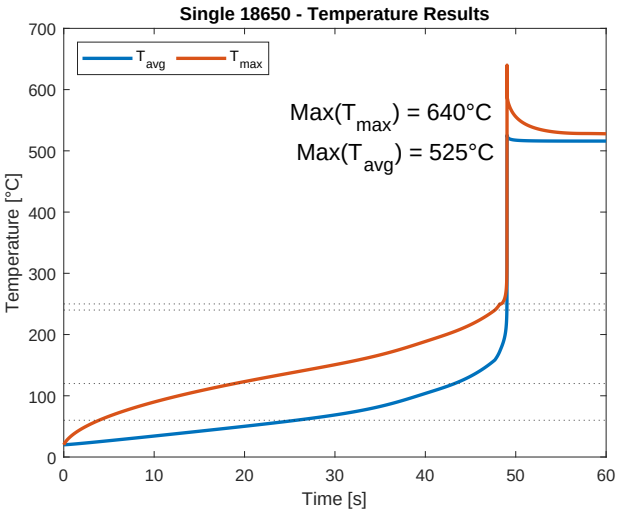

Figure 8: Temperature results recorded from the 18650 model.

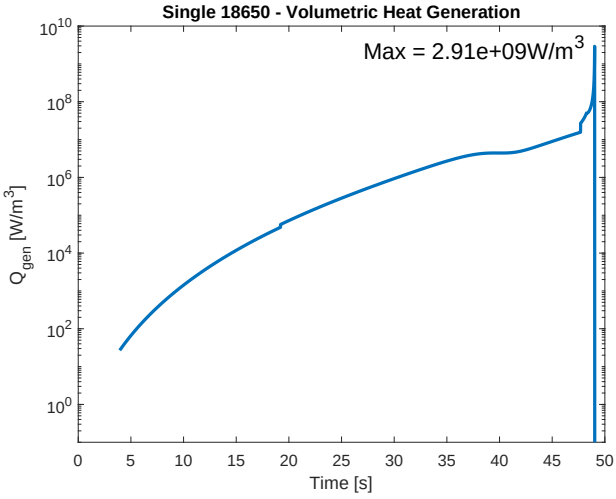

Figure 9: Volumetric heat generated from the decomposition reactions.

Figure 8 shows a gradual rise in battery temperature as the heater is active. The SEI is the first reaction to start at 60 °C, followed by the negative electrode at 120 °C, the positive electrode at 240 °C, and finally the electrolyte at 250 °C. While the heater does contribute to the initial temperature change of the battery, the decomposition reactions quickly become the dominant heat generation contributors. These reactions soon reach a critical point where a sharp increase in reaction rates are seen. This significantly increased reaction rate leads to the temperature and heat generation spike seen at $t \approx 49\,\text{s}$. The temperature quickly plateaus and approaches a steady-state value as no heat is lost to the environment and no reactant remains. The heater switches off at 240 °C, ensuring the only heat contribution is the decomposition reactions at the spike. This temperature spike would result in the battery catching fire and leading to the complete destruction of the battery. Multiplying the volumetric heat generation by the volume of the battery provides the total heat released from the battery shown in figure 12.

Figures 9–12 all show a characteristic sharp rise at $t \approx 49\,\text{s}$ followed by a sharp decline. This decline is

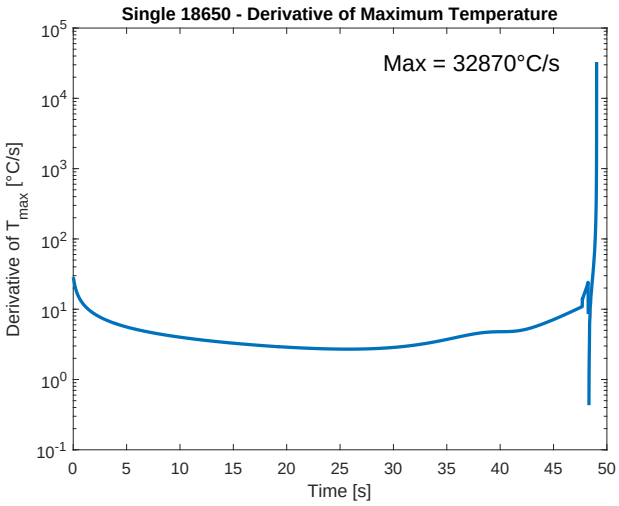

Figure 10: Maximum temperature rate of change

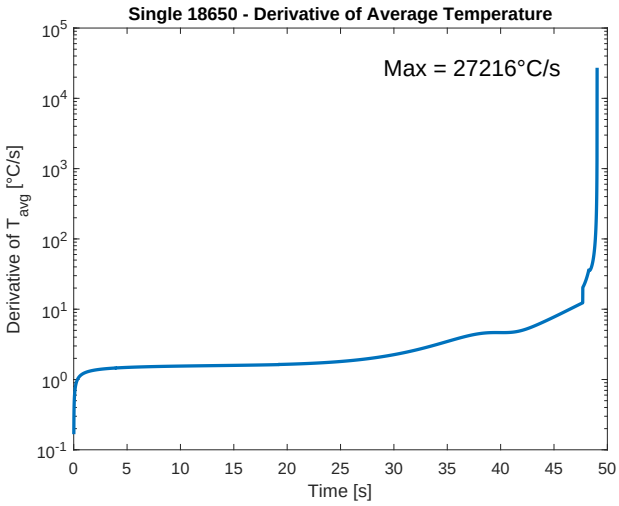

Figure 11: Average temperature rate of change

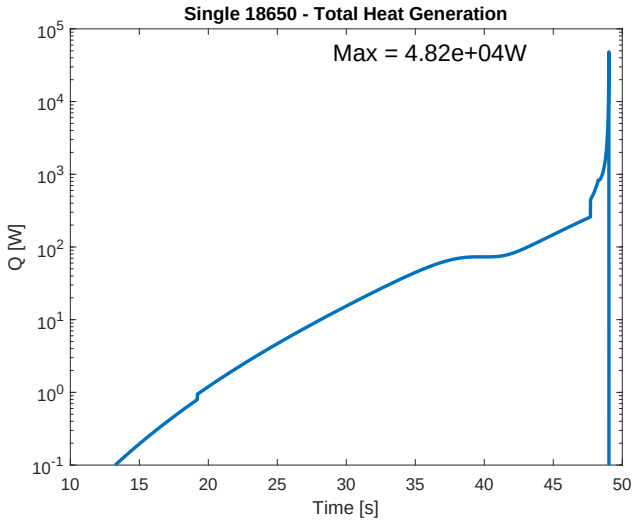

Figure 12: Total heat generation obtained from the volumetric heat generation data

not shown on the log plots as negative values are recorded after this point. The volumetric heat generation at this point jumps nearly two orders of magnitude over a few milliseconds as shown in figure 9. 13 shows the result of this significant heat generation. The entire battery temperature changes at this point until the battery and heater reach a steady state temperature. The maximum point of figure 9 marks the end of TR as the reactant is largely burned at this time, resulting in a sharp decline in Q_{gen}, but the temperature of the battery remains elevated. After $t \approx 50\,\text{s}$, the volumetric heat generation plot shows random noise which is largely bounded between $10^{-2}\,\text{W/m}^3$ and $10^{-5}\,\text{W/m}^3$. This contributes no practical change to the temperature of the battery and is therefore neglected after the spike.

The Q_{gen} values can be extracted and converted into a large piecewise function to obtain a heat generation function identical to figure 9. The single 18650 cell can now be converted into a volumetric heat source set

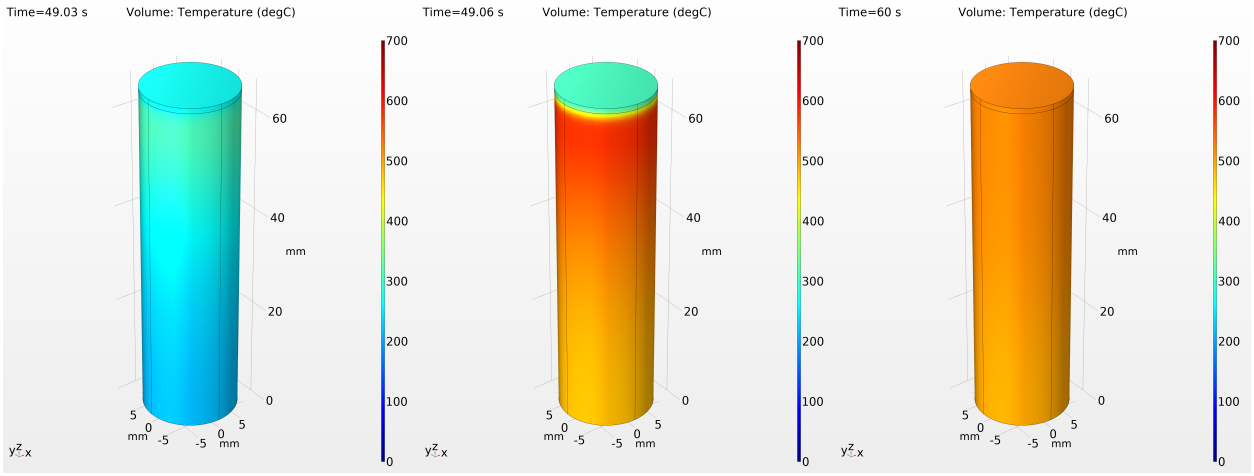

Figure 13: TR progression in the single 18650. From left to right: $t = 49.03\,\text{s}, t = 49.06\,\text{s}, t = 60\,\text{s}$

to output the piecewise heat generation function. This significantly reduces computation times as there is no longer a need to re-solve the differential decomposition reactions for future models. One limitation is the battery geometry, properties, and other parameters cannot change – it must remain an 18650 cell based on an $LiCoO_2$ cathode material. This is not an issue as this project only analyzes these types of LIBs. The input parameters shown in table 5 would need to be changed depending on the LIB chemistry selected for analysis.

This completed basis model can now be used in a generalized battery holder. This basis model serves as a trigger cell to evaluate methods to prevent the propagation of TR in multicell arrays.

3 The Honeycomb

3.1 Honeycomb Overview and Modeling

The honeycomb is the name given to the general battery holder design developed as part of this research. The basic configuration is shown in figure 14. It holds seven 18650-cells, all of which have the same material properties. Multiple honeycombs can be arrayed or stacked to obtain an arbitrary number of cells like in figure 16. This property is essential for high-power applications like electric cars or whole-house backup batteries which demand thousands of battery cells. Modeling the honeycomb considers some simplifications to ensure reasonable computation times. It is assumed the batteries inside the holder are in perfect contact with the walls of the case and transfer heat through conduction only. The top and bottom surfaces of the case and the batteries are allowed to lose heat through convection and radiation, so the total heat loss in

the system is

$$-\mathbf{n}\cdot\mathbf{q} = h(T_{\text{ext}} - T) + \varepsilon\sigma\left(T_{\text{amb}}^4 - T^4\right) \tag{12}$$

where T_{amb} is the ambient temperature, T_{ext} is the exterior temperature, and $\mathbf{n}$ is the normal vector of the surface. Both temperatures are initially set to $T = 20\,^{\circ}\text{C}$. The convective heat transfer coefficient, h, was set to $10\,\text{W/mK}$, while the surface emissivity, ε, was set to 0.7. These boundary conditions remain unchanged for all simulations involving the honeycomb. The dimensions shown in figure 14 remained unchanged as well. The center cell is the trigger cell for all tests unless stated otherwise, or if multiple trigger cells were used. Since the trigger cell is the exact same model described in section 2, the trigger cell in the honeycomb was turned into a heat source and outputted the Q_{gen} function seen in figure 9. This simplification bypasses solving the differential equations every time a new simulation is run. This greatly reduces runtimes and computer resource needs.

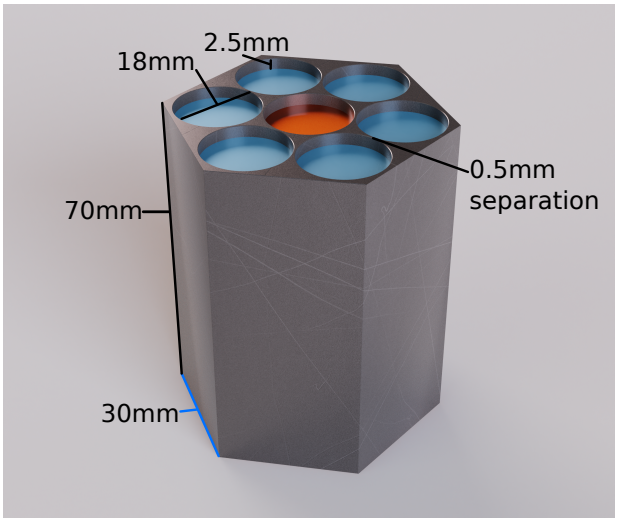

Figure 14: Unchanged honeycomb dimensions used for all studies.

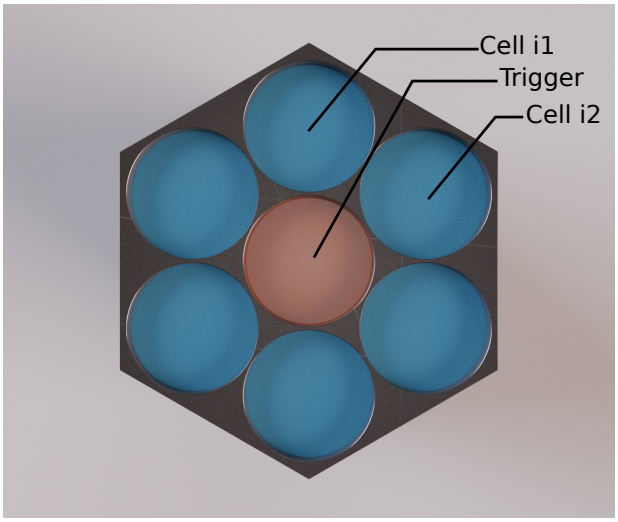

Figure 15: Cell arrangement: cells are named i1 to i6 going clockwise from cell i1, i7 is the trigger.

Data collected included the maximum and average temperatures seen in the trigger cell, the case, and the six surrounding cells. Since the center cell is modeled as a volumetric heat source, the temperature profile through the case will be largely radially symmetric. This means the maximum temperature seen in one of the surrounding cells will be close to the maximum temperature seen in the other batteries. The temperatures measured in cell i1 are reported to facilitate data comparison as labeled in figure 15. This eliminates the need to analyze all six battery temperatures, reducing analysis times as symmetry can be utilized. Since the model is radially symmetric, cell i1 corresponds to the cell at the hexagonal-geometry vertex furthest along the y-axis to maintain a consistent naming scheme. COMSOL shows the axes in the lower-left corner in figures like 17.

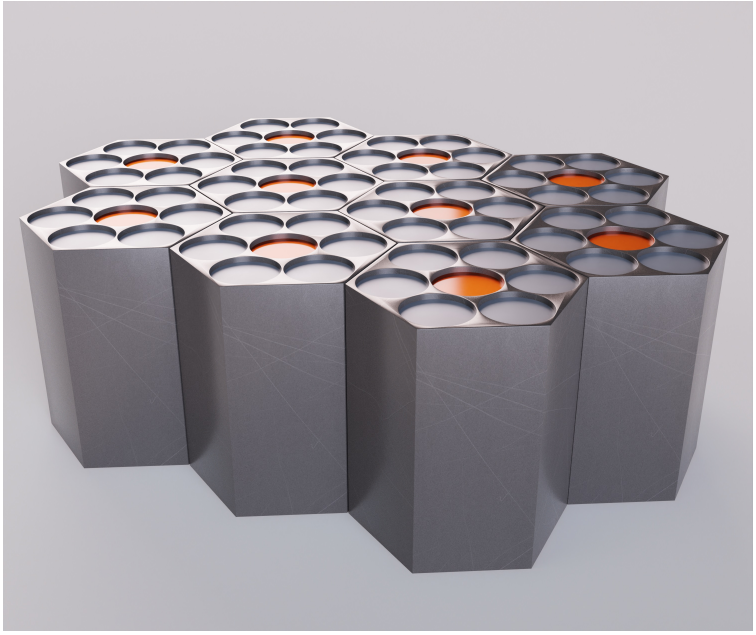

Figure 16: An array of honeycombs demonstrating scalability

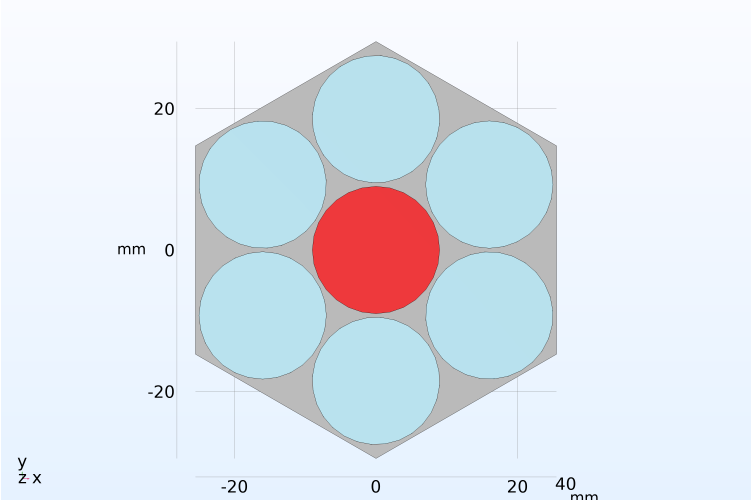

Figure 17: Top of honeycomb shown in COMSOL. Cell i1 is the topmost cell

A conservative failure criteria is assumed as well – this states if $T_{\max}$ of cell i1 exceeds 60 °C, the set of parameters imposed on the honeycomb has failed. The first decomposition reaction onsets at 60 °C, so it is assumed the TR process starts at this temperature, indicating the honeycomb failed to prevent TR propagation. While some heat is lost to the environment through the top and bottom surfaces, this is not enough heat removal once these reactions onset.

3.2 Analysis of Studies: Thermal Conductivity

Multiple properties of the honeycomb were varied to assess its ability to dissipate heat from the trigger cell. The first study analyzed the effects of thermal conductivity (k) on the model. The honeycomb material was set to Al-6063T83 which has the following base material properties: $\rho = 2700\,\mathrm{kg/m^3}$, $c_p = 900\,\mathrm{J/(kgK)}$ and $k = 201\,\mathrm{W/(mK)}$. Aluminum was chosen as it is a common material with a good strength to density ratio, variability in the types of alloys available, and in the case of Al-6063, high thermal conductivity. It was hypothesized that thermal conductivity would play the greatest role in heat dissipation. A higher k value should mean more heat energy is conducted away from the trigger cell and more quickly dissipated through the case and to the environment. This minimizes temperature hotspots and keeps the maximum temperatures in the case and surrounding batteries lower.

Nine values of k were chosen and nine simulations were run to determine trends in the honeycomb. No other properties were changed between simulations. The values of k were the following: 1, 5, 25, 50, 100, 200, 500, 1000, and 2000 W/(mK). This range covers a significant selection of materials from ceramics, through metals, and up to diamond. Some of these materials are highly impractical to use and are only considered to observe trends in the data. Figure 18 shows thermal conductivity and thermal diffusivity plotted on an Ashby chart for a broad range of materials. This visualizes to what material these values of k would correspond. If a suitable thermal conductivity value is selected, a new material for the case can be selected. However, this would also change density and specific heat, so results may fall outside the thermal conductivity trend slightly. This chart is beneficial for a later study analyzing specific materials.

The nine simulations were run in COMSOL and the following summarized data was obtained. It is not necessary to show all the results as only some data is needed to observe trends.

The maximum temperature of cell i1 and the honeycomb both decrease with increasing k as shown in figures 19 and 20. This follows since increasing thermal conductivity increases thermal diffusivity ($\alpha = k/(\rho c_p)$), which denotes increased heat movement in the honeycomb. This means heat is conducting away from the trigger cell and dispersing through the case quicker. This not only minimizes local temperature buildups, but it also allows more heat energy to reach the top and bottom surfaces of the case quicker, allowing some heat energy to dissipate to the environment. In the minimal k simulation, the temperature of the case was much higher than the temperature seen in the surrounding batteries. This relates to thermal diffusivity, as the low value of k means heat energy is not readily conducted through the material. Another important observation is the time it takes cell temperatures to drop. The plot of $T_{\mathrm{max,i1}}$ in the $k = 1$ case showed a sharp rise followed by a gradual but slow temperature decrease. In the $k = 1000$ case, the sharp rise is still there, but the temperature starts decreasing almost immediately after TR event termination. Not only

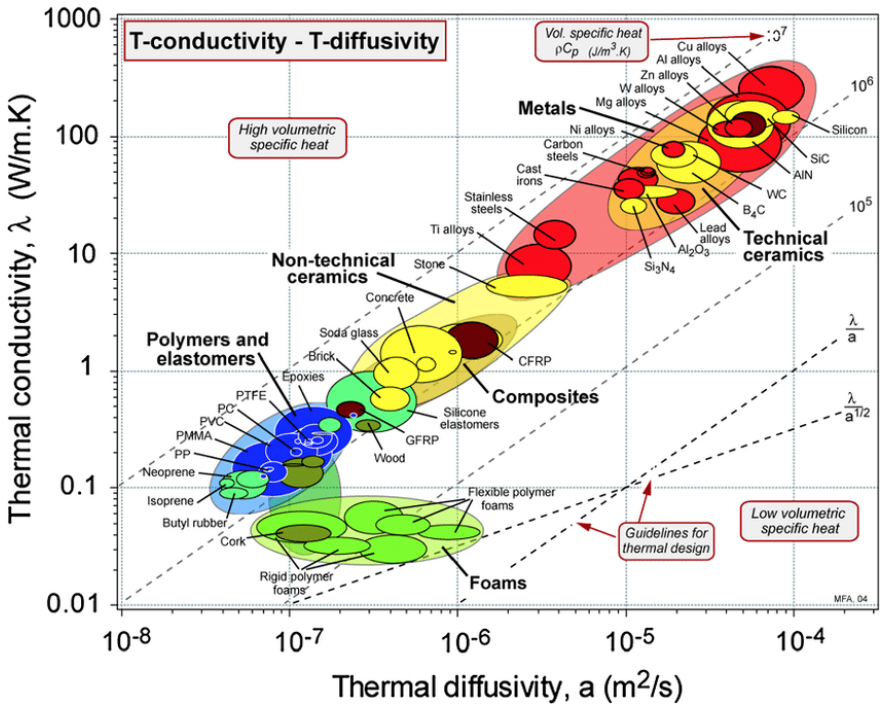

Figure 18: Ashby diagram showing thermal transport properties of various classes of materials [11]

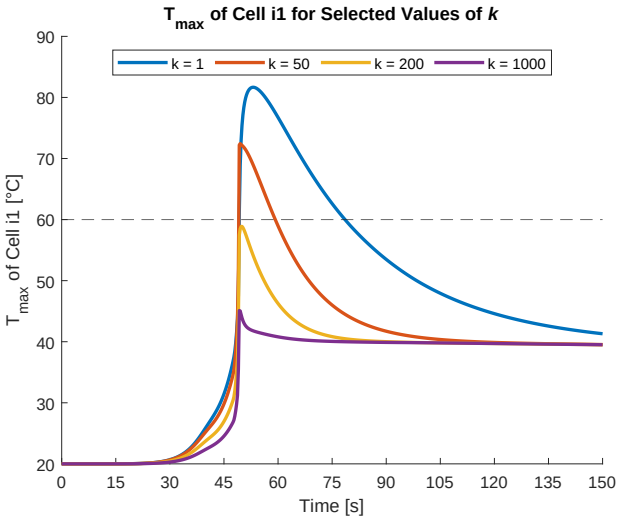

Figure 19: Maximum temperature results from cell i1 for selected values of k.

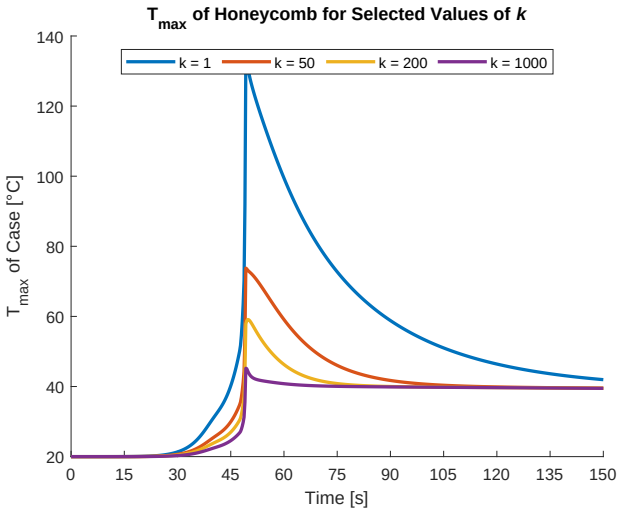

Figure 20: Maximum temperature seen in the honeycomb for selected values of k.

does increasing k lead to lower temperatures, but it also leads to these quicker cell temperature decreases. Plotting the maximum temperature seen in the nine simulations against k also reveals an exponential decrease in temperature with increasing k. The $k = 5$ case seems to break this trend, however, as the temperature of the cell in this simulation exceeded that of the $k = 1$ case.

A visualization of the temperature profile after TR onset is shown in figure 22. This figure shows three

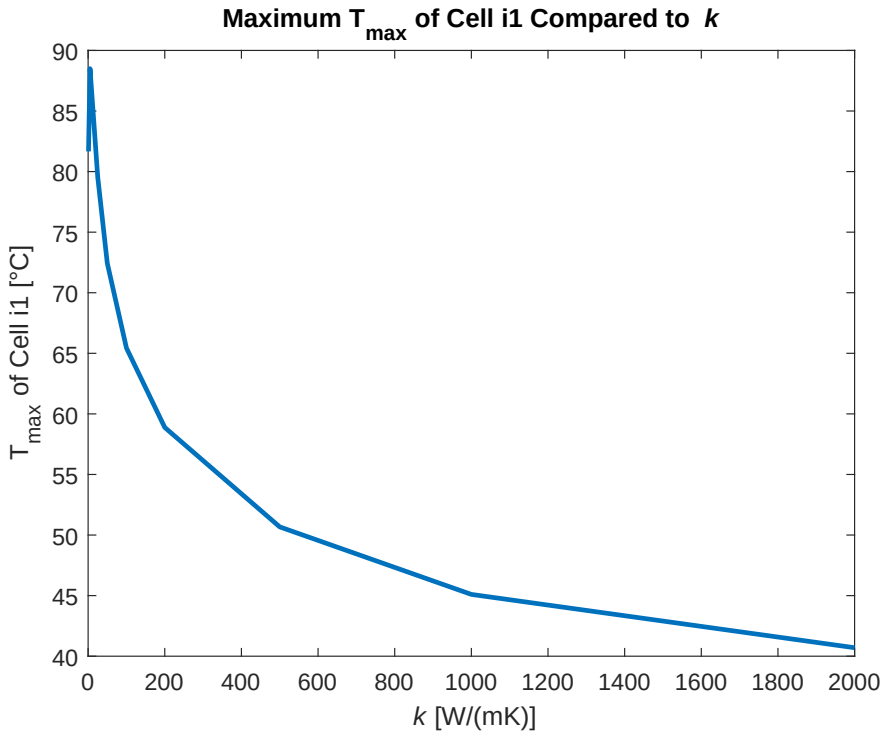

Figure 21: k compared to the maximum temperature seen in cell i1 in each simulation

honeycombs at $t = 55\,\mathrm{s}$ – the left honeycomb is set to $k = 1\,\mathrm{W/mK}$, the center is set to $k = 50\,\mathrm{W/mK}$, and the right honeycomb is set to $k = 200\,\mathrm{W/mK}$.

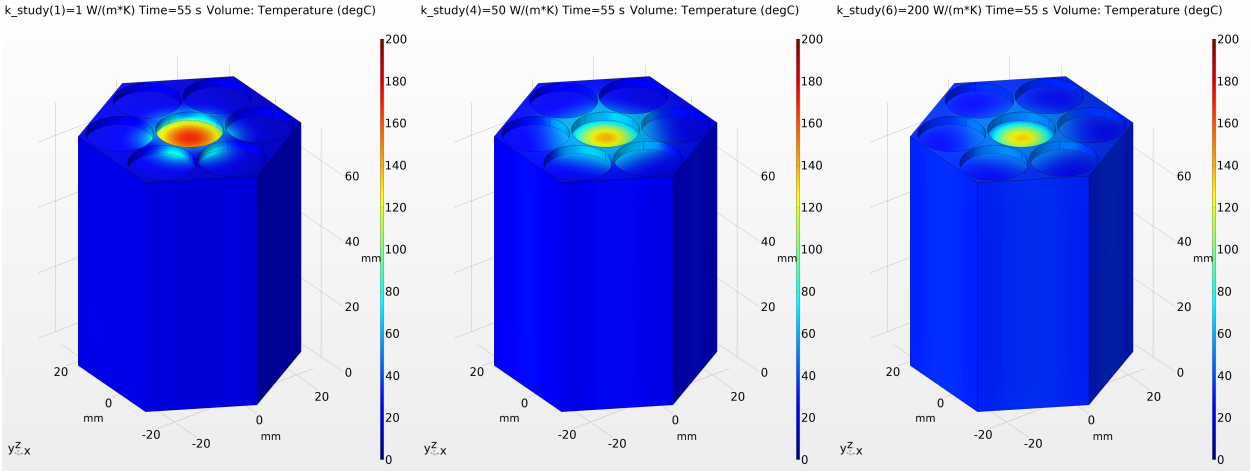

Figure 22: Temperature profiles seen in three honeycombs at $t = 55\,\mathrm{s}$ (left to right: $k = 1, 50, 200$)

The $k = 1$ (left) case in figure 22 shows localized hotspots along the inner edges of the cells. While most of the cell is still below the 60 °C threshold, these hotspots could trigger decomposition reactions in sections of the battery layers. These small reactions would only introduce more heat to the system, which could lead to another TR event in an outer cell. The other two cases show greater heat dispersion through

the case. The temperature buildups are more spread out in these cases, lowering the maximum temperature within those regions. Even though more heat energy may enter the cell due to increased heat dispersion, the temperature stays below the set TR onset temperature. This will prevent TR propagation as long as the 60 °C threshold is not exceeded.

3.2.1 Summary of k Study

The thermal conductivity study demonstrates that Al-6063, which has a value of k ranging from 201 – 218 W/(mK), may be a sufficient material for passively mitigating TR in a single-cell TR event. While this is a promising result, different applications will dictate material types, dimensions, and other parameters. Different events may trigger different cells or even multiple cells as well. This specific case shows results for one cell undergoing TR, but multiple trigger cells will have significantly varied results. It is also important to consider the simplifications made before. An electrically-insulating layer would normally be inserted between the battery and the case to prevent short circuits. This material would also affect heat transfer from the battery to the wall in practical applications. Instead, the honeycomb is modeled assuming perfect contact between the battery walls and the case itself. This would represent a worst-case scenario where the trigger cell releases a significant amount of energy into the case. The trends seen here are merely guidance to allow informed decisions on what materials may be most effective. An Ashby chart such as the one shown in figure 18 can be used to choose a material based on this study. Aluminum alloys, which generally have higher thermal conductivities than most other materials, would be a practical choice for fabricating honeycombs based on this study.

3.3 Analysis of Studies: Different Materials

This study analyzed the effects of different case materials on surrounding battery temperature. Unlike the thermal conductivity study where only the value of k varies, different materials affect density, heat capacity, and thermal conductivity. These all have varying effects on heat transfer within the honeycomb. Most of the materials selected were some form of metal as they would be the most realistic material to fabricate the honeycombs. Certain metals can provide good protection against TR, but they also provide a relatively strong structural element as well. This structural element may be necessary if honeycombs were installed in some application like an EV.

Table 4 shows the evaluated materials and their thermal properties. These materials have a wide range of densities, thermal conductivities, and specific heats. Each material has their benefits and properties making them more desirable than others for certain applications. For instance, magnesium is the least dense of

the materials tested while still providing good strength. While promising on paper, TR in a magnesium-based honeycomb could prove even more catastrophic than TR in LIB cells alone. A magnesium fire can very quickly engulf other cells, making this honeycomb material more detrimental than other materials. It is still evaluated for comparative purposes, however. Titanium is also a strong material for its density especially compared to many alloys of steel. Its low thermal conductivity means heat dissipation is much lower than other materials, however. These considerations are necessary when evaluating effective materials for honeycomb designs. The same testing procedure as the thermal conductivity study was also used for this study. One trigger cell was used, boundary conditions remain unchanged, but only the material changed from simulation to simulation. Figure 23 shows the temperature of cell i1 with some of these materials, while figure 24 shows the maximum temperature reached in the honeycomb.

	Density [kg/m^3]	Thermal Conductivity [kg/m^3]	Specific Heat [J/(kgK)]
Al-3003-H18	2730	155	893
Al-6063-T83	2700	201	900
Ti-B21S	4940	7.5	710
Copper	8960	400	385
Mg-AZ31B	1770	96	1000
High-strength Alloy Steel	7850	44.5	475

Table 4: Properties of materials chosen for testing

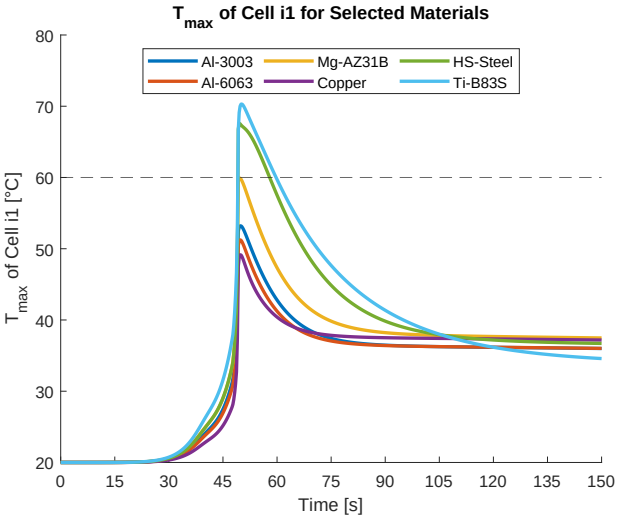

Figure 23: Maximum temperature results for cell i1 for selected materials

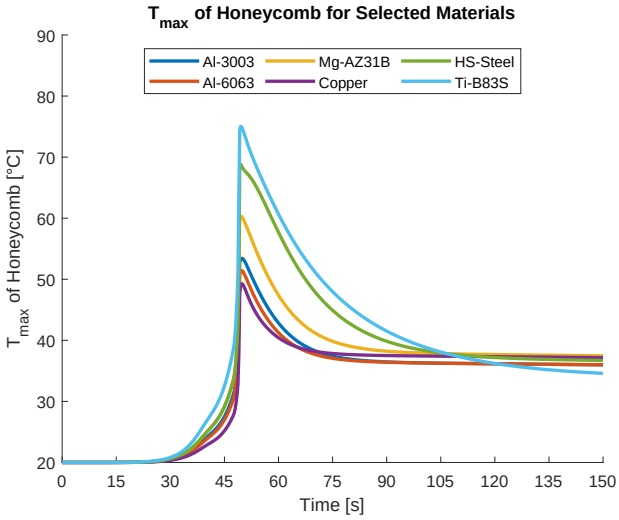

Figure 24: Maximum temperature results for the honeycomb for selected materials

Copper proved to be the best material for lowering the temperature of the outer cells, but Al-3033 and Al-6063 followed closely behind. The high thermal conductivity of copper most likely contributed to its

success in keeping cell temperatures low. However, copper is an impractical choice based on cost and weight. A design incorporating Al-6063 or another comparable alloy could prevent the temperature of the cell from reaching 60 °C. The general high-strength steel alloy and titanium proved ineffective against TR propagation. The low values of k in titanium and steel most likely led to its failure. This indicates thermal conductivity remains the dominant factor in thermal effects compared to density and specific heat. However, materials are not the only variable option in the model. It is also possible to vary other dimensions and conduct additional parametric studies.

3.4 Analysis of Studies: Cell Separation Distance

Parameterizing the honeycomb dimensions is necessary to conduct this study. This means defining all dimensions not in terms of numerical inputs but in terms of functions. One of these parameters is the cell separation distance defined as the shortest distance between two cells. Varying this dimension alters the side lengths of the honeycomb, so it is first necessary to define this side length as a function of battery size and cell separation. This allows parametric studies to be conducted while ensuring all dimensions are varied accordingly. This is done using equation 13. A demonstration of applying this equation is shown in figures 25 and 26.

$$\text{honeycomb side length} = d_{\text{batt}} + \frac{r_{\text{batt}} + \text{separation distance}}{\cos(30°)} + \text{separation distance} \tag{13}$$

It is also necessary to parameterize the location of the cells themselves. Only the position of the topmost cell needs to be defined since the other 5 can be placed using the "rotate duplicate" tool in COMSOL. The y-coordinate of this cell is simply d_{batt} + separation distance, and the other 5 cells are radially duplicated around the origin (0,0). This ensures symmetry is present in the model and all the cells are in the correct locations.

The parametric study can now take place. d_{batt} and r_{batt} are based on an 18650 cell, and separation distance is varied between between 0.5 mm and 11 mm at 1.5 mm increments. This resulted in 8 total simulations. The material was set to Al-6063 for this study and remained unchanged. An analysis similar to the thermal conductivity study was then performed.

Figures 27 and 28 show the results for the maximum temperature seen in cell i1 and the trend of temperature vs. separation distance. Another exponentially-decreasing trend was seen similar to the thermal conductivity study. Increasing the cell separation distance by just millimeters can reduce cell temperatures by a significant amount. Increasing the separation distance from 0.5 mm to 2.0 mm, for instance, was able to reduce the cell temperature by $-23.6\,\%$.

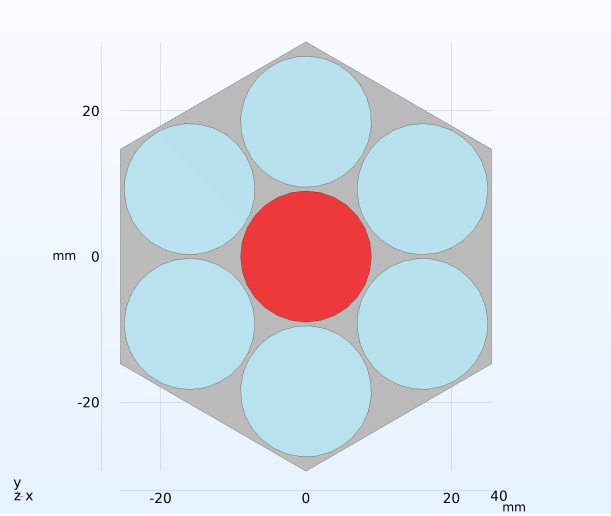

Figure 25: Honeycomb with 0.5 mm separation

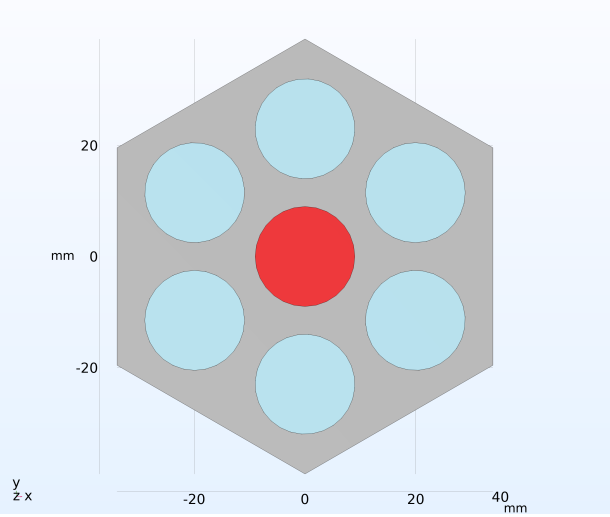

Figure 26: Honeycomb with 5 mm separation

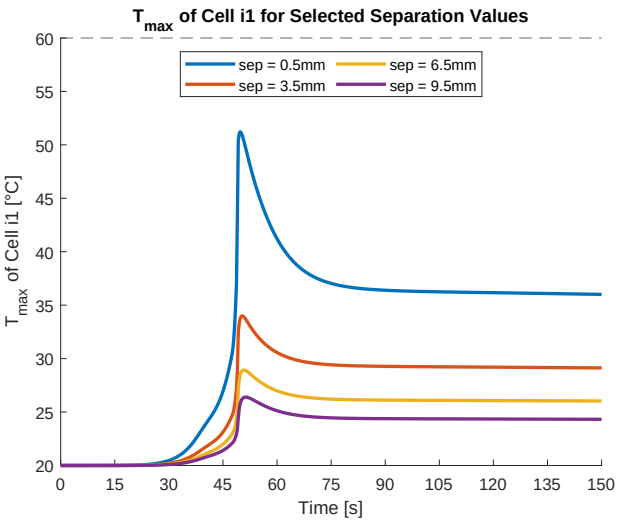

Figure 27: Cell temperatures with selected separation distances

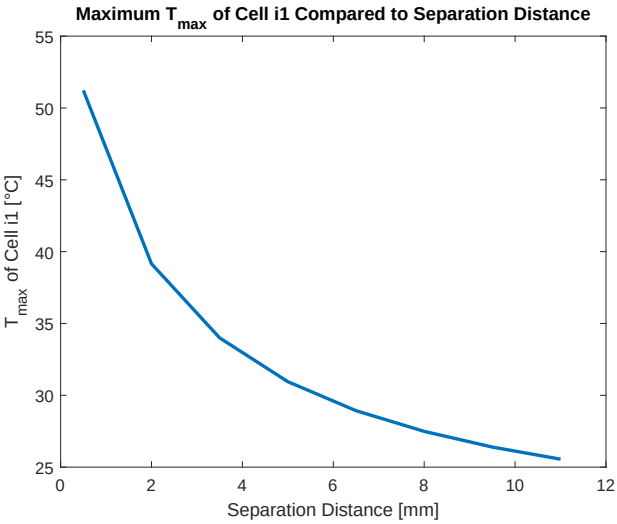

Figure 28: Trend seen in maximum temperatures vs. separation distance in cell i1

This study offers guidance on the general effects of increasing separation distance on the surrounding cell temperatures. Diminishing returns are present, so striking a proper balance between cell separation, weight, and resulting cell temperatures is necessary. The parameterization of the honeycomb also allows a quick estimate of the weight to be calculated. Since dimensions and materials are fully defined or provided, a function of the mass of the honeycomb was also found. While one honeycomb is light on its own, the combination of hundreds will add significant weight which must be accounted. This is especially important in EV applications which demand thousands of battery cells and therefore hundreds of honeycombs. Figure 29 shows the resulting mass function for the range of separation values in the conducted study. Figure 30 shows the mass function for a much wider range of separation values. This range of values captures the

exponential trend seen in mass as separation distance increases. Section 6 shows the weight calculation script in detail.

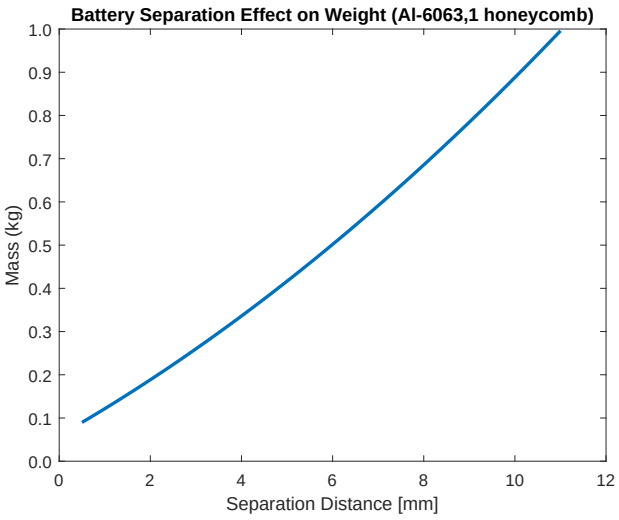

Figure 29: Battery separation distance effects on weight for a single honeycomb (provided range)

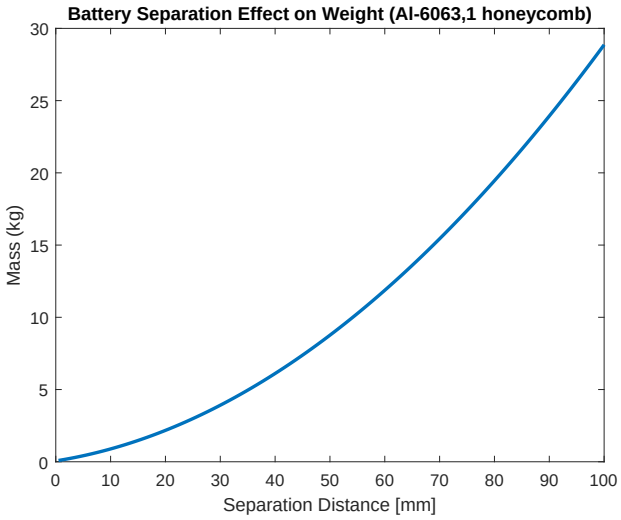

Figure 30: Battery separation distance effects on weight for a single honeycomb (wide range)

A practical example of weight calculation is based on the Tesla Model S "Plaid". This vehicles uses 7,920 18650 cells to supply the power necessary [4]. At a minimum, this equates to 1,132 honeycombs to hold all the battery cells. If Al-6063 were used as the honeycomb material, figure 31 is the resulting mass function with changing cell separation distance. The mass quickly increases with cell separation distance, especially when hundreds of honeycombs are necessary. This is another significant attribute to consider when selecting honeycomb parameters.

The need to balance material, cell separation distance, and safety become important. An EV needs to remain as light as possible to maximize range, but with thousands of battery cells, this can be a challenge. The models developed intend to help determine effects of materials, cell separation, and other parameters to ensure high degrees of safety in multicell arrangements. This study demonstrates how crucial this balance becomes.

3.5 Analysis of Studies: Multiple Trigger Cells

Another study analyzed the effects of multiple trigger cells in the honeycomb. This simulates a situation where an external stimuli simultaneously triggers TR in more than one cell. This results in additional heat generation within the honeycomb and presents another challenge to TR mitigation. Two tests were performed for this study: one with two trigger cells (figure 32) and the other with three (figure 33). While multiple combinations of trigger cells are possible, only these two are shown as numerous trigger arrangements are

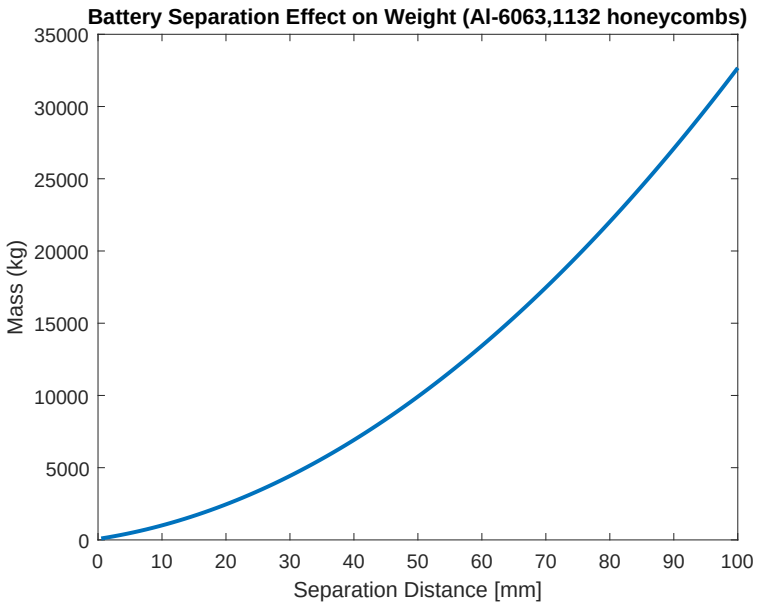

Figure 31: Mass of honeycomb function for a Tesla Model S Plaid

possible. The two trigger test evaluates an asymmetric situation where two nearby cells undergo TR while the three cell arrangement triggers every other outer cell. The material of the honeycomb was set to Al-6063 with the same material properties defined in 3.2. All cell temperatures were tracked and post-processing was performed to obtain data for the hottest cell only. The hottest cell will change depending on the arrangement of cells. As long as the hottest cell remains below the threshold temperature, the remaining cells will also remain under the temperature. The maximum temperature of the honeycomb is also reported.

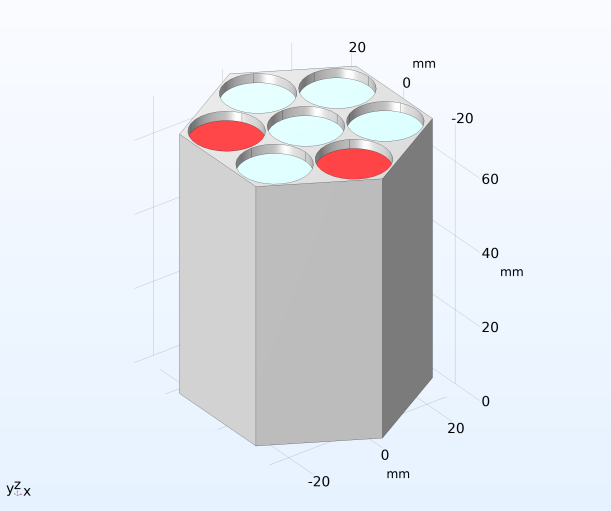

Figure 32: Two trigger cell arrangement

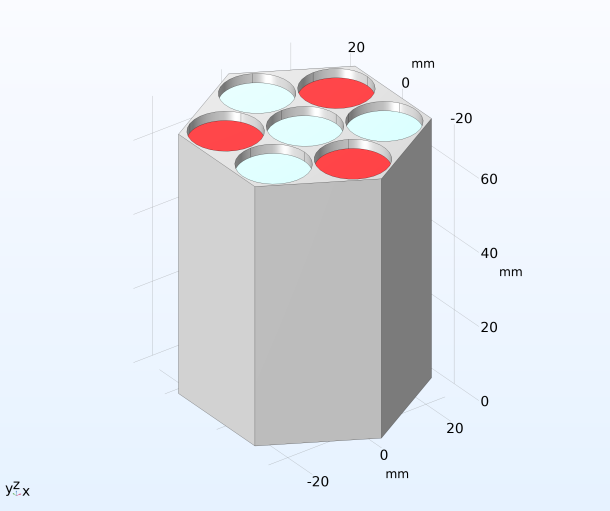

Figure 33: Three trigger cell arrangement

Figures 34 and 35 show these two data points plotted for the two cases. The two cell arrangement shows

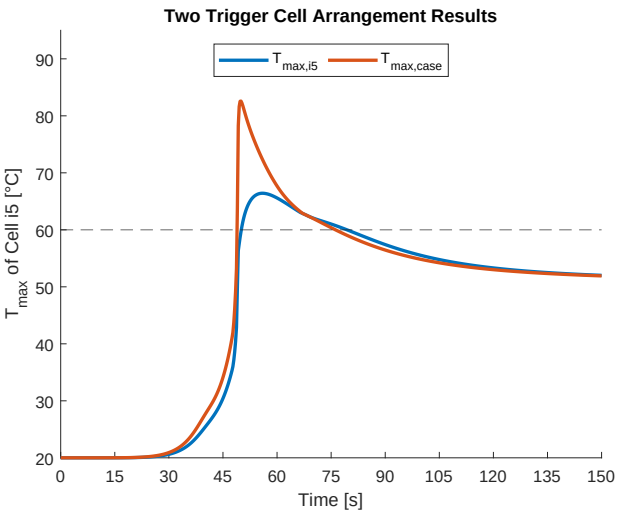

Figure 34: Relevant temperature results for the two trigger arrangement

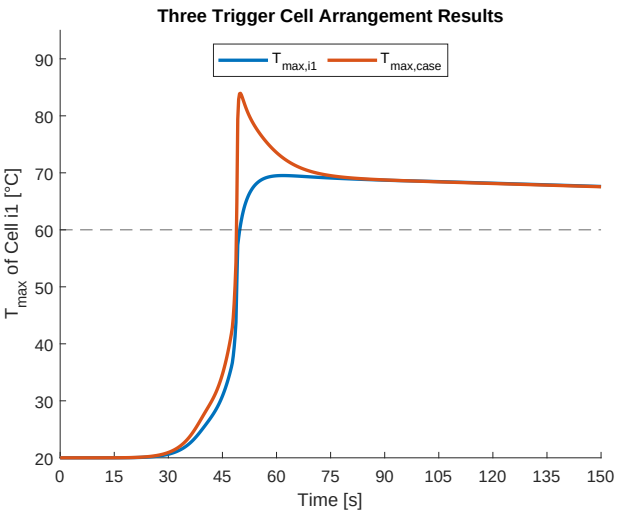

Figure 35: Relevant temperature results for the three trigger arrangement

results diverging from those seen previously. The asymmetry of the trigger arrangement means the case will take longer to reach a steady-state temperature since the triggers are more towards one side. This increases the time it takes for heat energy to dissipate throughout the entire geometry of the case and reach equilibrium. This results in the hottest cell temperature exceeding the cutoff temperature for roughly 40 seconds before dropping below it. The maximum temperature of the case and the cell are nearly coupled after this point as well. The plot depicting this shows an interesting result as it indicates TR can be prevented if some cooling method is applied quickly enough to keep the temperature below the maximum point. The battery eventually drops below 60 °C, so applying external cooling for a short duration can prevent TR from propagating. This would greatly increase complexity in this particular model, so this process is not simulated. However, one promising method by which to prevent TR propagating is increasing battery separation. This has been shown to have great effects on the cell temperatures, presenting one viable option.

The three cell arrangement does not reach temperatures much greater than in the two cell arrangement. The maximum temperature seen in the case is nearly equal, but after TR terminates is where differences start. Unlike the two cell arrangement, the temperatures level off more quickly and do not show a significant decrease. The cell temperature does not exhibit a significant decrease in temperature either. Both the case and the cell temperature are coupled after the 75 s mark and remain above the 60 °C cutoff. This signifies that the entire case is at this temperature and the remaining cells are also close to this temperature. This sustained temperature would cause TR to propagate in all the other cells, albeit rather slowly. This result is expected, as multiple triggers would release more energy into the case. Some parameter would need to be change to account for the extra heat energy.

These multicell triggers present a potentially catastrophic situation in which multiple batteries undergo TR simultaneously. These situations are more rare than a TR event normally is, but their consequences can be more catastrophic. Such an event could be onset due to damage to the entire honeycomb structure, inadequate cooling, or damage to the electrical components connected to the batteries. These simulations show how battery temperature can change when different trigger cell arrangements are evaluated.

3.6 Basic Force Testing

Physical damage serves as another potential trigger for TR. If an object punctures the case and damage a cell, an ISC may result followed by TR initiation. A force loading on the case can also trigger TR through the same mechanisms. Deformations in the honeycomb can force the internal layers of certain cells to contact one another and cause an ISC – effectively triggering TR through by crushing the battery. This necessitates the need to study basic loading conditions on the honeycomb to determine effects of forces. This data can provide insight to where maximum deformations occur in the honeycomb structure. These tests are conducted in 2D instead of 3D as in the thermal evaluations. A 2D setup simulation allows quick "order of magnitude" testing of multiple honeycombs joined together. Running the simulation in 3D greatly increases the number of meshing elements required to obtain a proper solution. 3D is also unnecessary in the case of a constant pressure force since the deformation through the depth of the case is largely constant. 2D also allows much larger honeycomb structures to be modeled without a significant increase in the number of meshing nodes required for accurate results.

The first basic test involved joining three honeycombs together as shown in figure 36. The battery cells are removed so only the honeycomb structure itself is analyzed. This allows a 2D simulation to proceed as the cross-section area of the honeycomb is constant throughout its depth. A simple, increasing pressure force is applied to the upper surfaces acting in the direction of the red arrows shown. The pressure function is simply $F = 5t$ where F is the applied pressure force in PSI and t is the simulation time in seconds. The simulation runs from $t = 0\,\text{s}$ to $t = 600\,\text{s}$ and then rests for $30\,\text{s}$ after. This means the pressure force varies from $0\,\text{PSI}$ to $3,000\,\text{PSI}$ over the duration of the simulation. The downward-facing surfaces are fixed, simulating a case where the honeycombs are installed in a specially-fitted holder. This test focuses on what magnitude and locations of deformations seen within the case. An animation was generated to see how deformation progresses with time, and the last time step ($t = 630\,\text{s}$) is shown in figure 37. Displacement magnitudes overlaid with the displacement field are shown – this corresponds to a pressure force of $3,000\,\text{PSI}$.

The simulation is run using Al-6063 as the default material and the default dimensions described in section 3. The height of the honeycomb is only considered in the force calculations but not in the actual

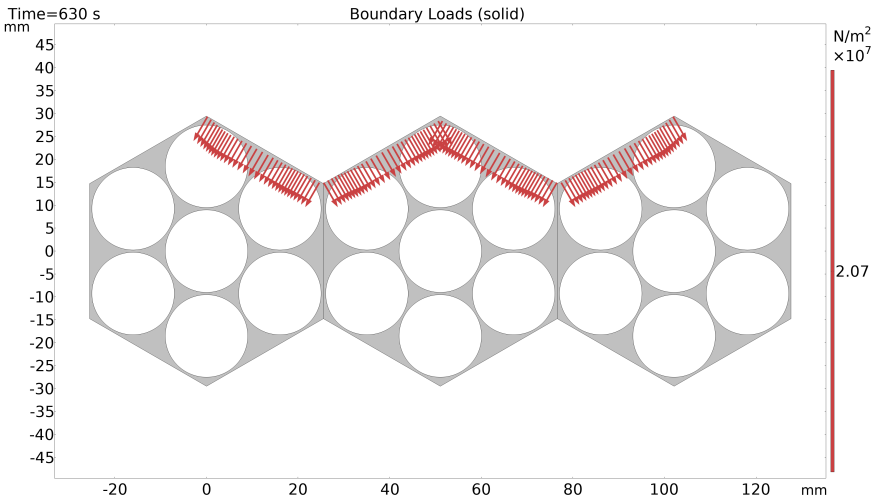

Figure 36: Boundary conditions for force testing

geometry itself. This greatly reduces computation time while still considering the honeycomb dimensions.

Figure 37 shows the magnitude of displacement at the final time in the simulation. Maximum deformations were seen in the topmost cell of the right and left honeycombs. Cells inserted into these boreholes could have their inner layers crushed together leading to an ISC. However, $3,000\,\text{PSI}$ is a rather significant loading which would most likely not be experienced in many applications. Increasing the cell separation distance would increase strength as well, but this also comes at a cost of added mass. The three honeycomb arrangement shown can resist significant deformations rather well even up to $3,000\,\text{PSI}$. Adding more honeycombs in the array would simply duplicate the deformation pattern seen, so this is not necessary to compute. Deformations are further minimized when the honeycombs are held together on the left and right sides of the structure. If a honeycomb arrangement were installed into a tough, reinforced case, it could help to further mitigate these deformations. This is especially important for EVs, where the honeycomb must handle the forces of driving, potential collisions, and other unforeseen events. While this force test serves as a simple starting point, further studies will need to be conducted for different applications, honeycomb arrangements and parameters, and material properties.

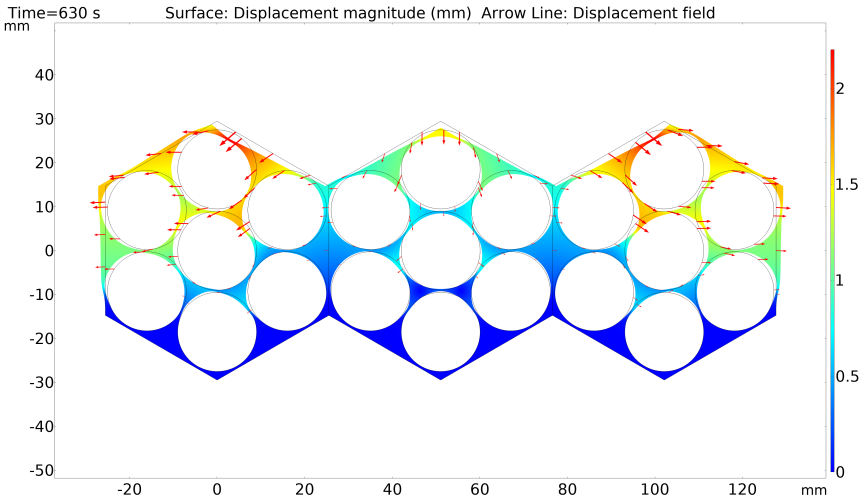

Figure 37: Deformations seen at maximum force application

4 Closing Remarks

4.1 Summary

This research saw the completion of an 18650 cell undergoing TR with a LCO cathode. Temperature and volumetric heat generation data were recorded and provided insight into the TR process. While the timing of specific reactions changes depends on battery chemistry and even manufacturing variability, the magnitudes of the temperatures and heat generation recorded are still relevant. The success of triggering TR in a single cell led to the development of a generalized battery holder called the honeycomb. The basis 18650 trigger cell model was then fit into the honeycomb and evaluated against different material properties, varying dimensions, trigger cell arrangements, and others. Changing these parameters allows insight to how materials or other parameters can affect propagation of TR in the honeycomb. Temperature data can be obtained, trends can be observed, and informed decisions can be produced based on results. The trends and results can be used to select potential materials for use in fabrication. Further testing can evaluate how the honeycomb handles applied forces, pressures, and other external loads.

4.2 Conclusions

The two primary objectives outlined at the beginning of the research were met. Objective 1 required the development of a basis model in which TR can be triggered. This was achieved using an 18650 form factor with the relevant decomposition reactions. The second objective required the development of a generalized battery holder which could mitigate TR effects. The varying nature of this particular study allowed for multiple studies to be conducted. Material properties were the primary focus, with additional tests including different honeycomb materials and trigger cell arrangements.

Modeling this phenomenon was a significant undertaking in COMSOL. No exact module for modeling heat generation by decomposition exists within COMSOL, so the heat generation equations needed to be input manually. The numerical nature of the project means results will not align perfectly with experimental trials or literature. The analytical functions describe a perfect model, which is not the case in real-world applications. Understanding what simplifications could be made were necessary as well. These simplifications and assumptions allow simulations to compute in a reasonable time at the cost of some accuracy. These simplifications, however, do not affect how the decomposition reactions were solved, so there is high confidence the heat generation terms are solved correctly.

A tertiary objective not originally outlined involved analyzing the honeycomb under basic loading conditions. This testing provided information as to where points of deformation exist within the honeycomb.

This is important for applications where the honeycomb would experience harsher conditions such as in an EV. Stationary setups do not need to account for forces as much as mobile applications, however. Knowing locations of these deformations are important, as physical damage to batteries presents another opportunity for TR to onset. Therefore, it is important that the honeycomb not only protect against thermal effects, but also physical effects.

The honeycomb provides a good basis off which TR mitigation techniques can be developed. This is crucial for improving battery safety across a number of applications. With demand of LIB only increasing over the next decade, it is imperative safety is considered before the rapid proliferation of batteries continue. The honeycomb and associated simulations provide a significant starting point off which multicell arrays can be modeled quickly. Material properties and other parameters can be varied to see their effects.

4.3 Future Work and Guidance

The 18650 basis model can be readily incorporated into other models to assess mitigation methods as was done in this research. If the honeycomb model is to be used, multiple trigger cells, additional honeycomb parametric studies, and varying dimensions should be assessed to see how TR propagates in such cases. Different applications will dictate these parameters. The numerical nature of this study means the results shown should be taken as guidance and not an exact solution as is the case with any FEA simulation. Different applications will dictate what dimensions, materials, and other parameters can be applied to the honeycomb. For applications where weight matters, other properties such as porous materials are being explored. A material such as porous aluminum can significantly reduce weight, but also ensure the internal cells are protected against thermal and physical damage. Other battery chemistries and sizes will be explored as well to see if there are noticeable impacts on thermal behavior in the honeycomb.

Once a known application is needed, a decision for materials, dimensions, and other parameters for the honeycomb should be decided. It is recommended one parameter is considered at a time, however. This allows for parametric studies to be done, which can be essential for finding optimal values of certain properties. This has the indirect effect of reducing material or manufacture costs should the honeycomb hypothetically be manufactured. Multiple trigger cells can also be incorporated to assess how the honeycomb will handle multiple cells undergoing TR simultaneously. Different scenarios can be evaluated with this approach. The default honeycomb files record the maximum and average temperatures of all the cells and the honeycomb itself, so this data can be post-processed to assess performance. Changes can then be made as needed.

5 Bibliography

[1] Flash Battery Safety - Nail Penetration Test. Flash Battery, 2019.

[2] F. Richter, “Infographic: High demand for lithium-ion batteries,” Statista Infographics, 18-Dec-2020. [Online]. Available: https://www.statista.com/chart/23808/lithium-ion-battery-demand/.

[3] Global Energy Storage Market set to hit one terawatt-hour by 2030. BloombergNEF. (2021, November 10). Retrieved from https://about.bnef.com/blog/global-energy-storage-market-set-to-hit-one-terawatt-hour-by-2030/

[4] Kane, M. (2021, October 13). Watch Tesla Model S Plaid’s Battery GET opened and described. InsideEVs. Retrieved from https://insideevs.com/news/540380/tesla-models-plaid-battery-open/

[5] L. Zhang et al, "A Computational Study on the Critical Ignition Energy and Chemical Kinetic Feature for Li-Ion Battery Thermal Runaway," SAE Technical Paper, vol. 2018-01-0437, 2018. DOI: https://doi.org/10.4271/2018-01-0437

[6] L. Zhang, P. Zhao, M. Xu, and X. Wang, “Computational identification of the safety regime of Li-ion Battery Thermal Runaway,” Applied Energy, vol. 261, 2020.

[7] M. Zhang, J. Du, L. Liu, A. Stefanopoulou, J. Siegel, L. Lu, X. He, X. Xie, and M. Ouyang, “Internal Short Circuit trigger method for lithium-ion battery based on shape memory alloy,” Journal of The Electrochemical Society, vol. 164, no. 13, 2017.

[8] N. Bullard, “This Is the Dawning of the Age of the Battery,” 17-Dec-2020. [Online]. Available: https://www.bloomberg.com/news/articles/2020-12-17/this-is-the-dawning-of-the-age-of-the-battery?srnd=green.

[9] P. T. Coman, E. C. Darcy, C. T. Veje, and R. E. White, “Numerical Analysis of heat propagation in a battery pack using a novel technology for Triggering thermal runaway,” Applied Energy, vol. 203, 2017.

[10] Q. Li, C. Yang, S. Santhanagopalan, K. A. Smith, J. Lamb, L. A. Steele, and L. Torres-Castro, “Numerical Investigation of Thermal Runaway Mitigation through a Passive Thermal Management System,” Journal of Power Sources. [Online]. Available: https://www.osti.gov/pages/servlets/purl/1512670.

[11] Revisiting the first Sandia Fracture Challenge with transient deformation heating and strain localization considerations - Scientific Figure on ResearchGate. Available from: https://www.researchgate.net/figure/Ashby-diagram-showing-thermal-transport-properties-of-various-classes-of-materials_fig_346267763

[12] S. Wilke, B. Schweitzer, S. Khateeb, and S. Al-Hallaj, "Preventing thermal runaway propagation in lithium ion battery packs using a phase change composite material: An experimental study," Journal of Power Sources, vol. 340, pp. 51–59, 2017.

6 Appendix A: Input Parameters

These parameters are used for the decomposition reaction and heat generation functions. They are used only for LIBs with an LCO cathode material.

Variable	Value	Units	Label
A_{sei}	1.66×10^{15}	[1/s]	SEI decomposition frequency factor
A_{ne}	2.5×10^{13}	[1/s]	Negative electrolyte frequency factor
A_{pe}	6.667×10^{13}	[1/s]	Positive electrolyte frequency factor
A_{e}	5.14×10^{25}	[1/s]	Electrolyte decomposition frequency factor
$E_{\text{a,sei}}$	1.3508×10^{5}	[J/mol]	SEI decomposition activation energy
$E_{\text{a,ne}}$	1.3508×10^{5}	[J/mol]	Negative electrolyte activation energy
$E_{\text{a,pe}}$	1.3508×10^{5}	[J/mol]	Positive electrolyte activation energy
$E_{\text{a,e}}$	1.3508×10^{5}	[J/mol]	Electrolyte decomposition activation energy
α_0	0.04		Initial value for α
$c_{\text{sei,0}}$	0.15		Initial value for c_{sei}
$c_{\text{ne,0}}$	0.75		Initial value for c_{ne}
$c_{\text{e,0}}$	1		Initial value for c_e
m_{sei}	1		Reaction order for SEI
$m_{\text{ne,0}}$	1		Reaction order for NE
$m_{\text{pe,p1}}$	1		Reaction order for α
$m_{\text{pe,p2}}$	1		Reaction order for $(1-\alpha)$
m_e	1		Reaction order for electrolyte
$t_{\text{sei,0}}$	0.033		Initial value for t_{sei}
H_{sei}	2.57×10^{5}	[J/kg]	Specific enthalpy of SEI
H_{ne}	1.174×10^{6}	[J/kg]	Specific enthalpy of NE
H_{pe}	3.14×10^{5}	[J/kg]	Specific enthalpy of PE
H_{e}	1.55×10^{5}	[J/kg]	Specific enthalpy of electrolyte decompositon
W_c	6.104×10^{2}	[kg/m^3]	Specific carbon content in jellyroll
W_p	1.221×10^{3}	[kg/m^3]	Specific positive active content in jellyroll
W_e	4.069×10^{2}	[kg/m^3]	Specific electrolyte content in jellyroll
R_u	8.314	[J/mol·K]	Universal gas constant
T_{amb}	293.15	[K]	Ambient temperature
Q_{in}	1.18×10^{9}	[W/m^3]	Volumetric heat input

Table 5: Table of variables used for the TR model in COMSOL – these values are for an LCO LIB

Appendix B: Weight Calculation

Below is a MATLAB script used for calculating the mass of a honeycomb. An input material density and number of required battery cells is inputted. The number of honeycombs is determined from the cell number input. The calculation assumes the honeycomb is solid, and that the boreholes into which the battery are fitted extend throughout the geometry. The script then outputs the minimum number of honeycombs and a plot showing the mass of all the honeycombs as a function of battery separation distance.

```
clear variables; clc

u = symunit();
line = 2;

% calculating for 18650 cell
r_batt = 9 * u.mm;
h_batt = 65 * u.mm;
vol_batt = pi * r_batt^2 * h_batt;

rho = input('Input density of material [kg/m^3]: ') * u.kg/u.m^3; % honeycomb density
h_hc = input('Height of honeycomb [mm]: ') * u.mm; % honeycomb height
sep = linspace(0.5,100,100) * u.mm; % separation distances at which to calculate weight
n_hc = ceil(input('Number of battery cells required: ')/7); % minumum honeycombs required

hc_side_length = (2 * r_batt) + (r_batt + sep)/cos(pi/6) + sep; % honeycomb side length
vol_hc = (h_hc * (3*sqrt(3)/2) * hc_side_length.^2) - 7*(pi * r_batt^2 * h_hc);
mass_hc = n_hc * unitConvert(vol_hc .* rho, 'SI');

% outputs
fprintf('Number of honeycombs required: %1.0f\n', n_hc*7, n_hc);
plot(separateUnits(sep),separateUnits(mass_hc),'LineWidth',line)
xlabel('Separation Distance [mm]')
ylabel('Mass (kg)')
if n_hc == 1
```

```
26      title(strcat('Battery Separation Effect on Weight (Al—6063, ', num2str(n_hc), '
            honeycomb)'))
27  else
28      title(strcat('Battery Separation Effect on Weight (Al—6063), ', num2str(n_hc), '
            honeycombs)'))
29  end
```